

A Stimulus-Response Based EEG Biometric using Mallows Distance

Baicheng Chen¹ · Kun Woo Cho² · Chenhan Xu¹
Zhengxiong Li¹ · Feng Lin³ · Zhanpeng Jin¹ · Wenyao Xu¹

Received: date / Accepted: date

Abstract Electroencephalogram (EEG) activity from the brain is a promising biological marker that can serve as personal identification. Despite substantial efforts, it remains an unsolved problem to quantify EEG feature distribution for brain biometrics due to the complexity of the brain. In this study, we attempt to tackle EEG-based identification challenges by exploiting a novel distribution model. The distribution dissimilarity is measured by Mallows distance, a cluster similarity sensitive distance that is robust to signal noises. Specifically, EEG signals are decomposed through several statistical feature extraction methods, autoregressive (AR) model, discrete wavelet transform (DWT), and fast Fourier transform (FFT). With the dataset obtained from the real-world application, our proposed system achieves the f -score accuracy of 96.18% and half total error rate of 2.223%, which demonstrates the feasibility and effectiveness of utilizing EEG biometrics for personal identification applications.

Keywords Biometrics · Secure Authentication · Wearable Computing

1 Introduction

Personal Identification has been a long-lasting problem around the world. Due to the large population of humans, existing methods often fail with a lack of identification accuracy in

system design. Researchers are actively attempting to solve this problem, yet, solutions often compromise quickly due to the computational complexity and performance speed trade-off. In wearable computing application scenarios, authentication methods with high computational complexity require a longer time, while rapid authentications are often quickly reverse-engineered. In the past decades, the technique of using biometrics for personal identification to secure information has gained massive popularity (Jain et al., 2008; Tian et al., 2018). Anthropocentric traits are now playing pivotal roles in everyday user authentication for both privacy and security purposes. From authenticating a user through fingerprint, face or iris, banking service authentication using voice, medical analysis using gait, to governmental agency utilizing DNA toward citizen identification (Jain et al., 1997; Beenau et al., 2006; Raja et al., 2015; Brumback et al., 2015), biometric applications cover a wide variety of scenarios. Moreover, innovative biometric modalities, including palm vessel (Li et al., 2018; Wang et al., 2018), heartbeat (Lin et al., 2017; Zhuang et al., 2016; Zhang et al., 2020), eye movement (Song et al., 2016; Luo et al., 2019), sonic fingerprint (Rathore et al., 2020), and pulse (Patil et al.,

Baicheng Chen
E-mail: baicheng@buffalo.edu
Kun Woo Cho
E-mail: kwcho@princeton.edu
Chenhan Xu
E-mail: chenhanx@buffalo.edu
Zhengxiong Li
E-mail: zhengxio@buffalo.edu
Feng Lin
E-mail: flin@zju.edu.cn
Zhanpeng Jin
E-mail: zjin@buffalo.edu
✉ Wenyao Xu
E-mail: wenyaoxu@buffalo.edu

1 University at Buffalo, the State University of New York, Buffalo, New York, USA

2 Princeton University, Princeton, New Jersey, USA

3 Zhejiang University, Hangzhou, Zhejiang, China

2018), are recently investigated with promising performance. The advancement of biometrics provides tremendous security and safety benefits to civilians.

Among existing anatomical and behavioral biometrics, the EEG signal is one of the metrics related to individual-specific human characteristics. It has newly emerged as a resource for biometric-based personal identification. The human brain is highly complex and dynamic as it operates information at high speed and quantity; this results in EEG signals acquired from the brain also being highly complex and dynamic. The complexity of comprehension adds a level of security in terms of being less prone to spoofing and counterfeiting attacks. Compare to other biometric techniques such as DNA testing and gait analysis, the recording of EEG signals is non-invasive and non-dispersal, which significantly reduces user discomfort as well as prevents an attacker from EEG response pilfering. Therefore, it is highly feasible to replace currently existing biometric identification methods based on DNA, fingerprint, voice, gait, and iris (Poulos et al., 2002; Gui et al., 2015b, 2014a) with EEG in personal identification applications.

1.1 Related Work

Existing EEG biometric personal identification work mostly focused on the classification of pathologically induced EEG signals, which can have high uncertainty and abnormalities with the occurrence of severe psychiatric disorders, such as epilepsy or schizophrenia (Hazarika et al., 1997; Juel-Nielsen and Harvald, 1958).

Nevertheless, the success in distinguishing pathological EEG signals from a healthy subject using particular signal analysis methods like discrete wavelet transform and fast Fourier transform demonstrates that specific variations in the EEG pattern can serve as a good resource for a non-clinical personal identification (Hazarika et al., 1997; Ocak, 2009; Subasi, 2007). In addition, EEG signal from healthy subjects has been validated by several studies in the past. For instance, Poulos *et al.* presented the person identification using EEG of healthy individuals by implementing a set of non-linear model parameters as a feature of the EEG signal. This model was then classified by an artificial neural network classifier. Although the classification accuracy of the method was not high enough (76 – 88% for accuracy) for the direct implementation of EEG identification, their results prove that the EEG can be successfully exploited for subject identification (Poulos et al., 2002).

Similarly, Mohammadi *et al.* proposed a personal identification using the autoregressive model for EEG signals and achieved the classification score in the range of 80 – 100% (Mohammadi et al., 2006). Gui *et al.* studied a set of event-related potential patterns to identify users (Gui et al., 2015c, 2014b, 2015a). Recently, Lin *et al.* applied brain biometrics

in wearable and mobile applications for secure user authentication (Lin et al., 2018).

1.2 This Work

In this work, we present a stimulus-response based EEG personal identification mechanism using Mallows Distance to compute EEG feature distribution distance. One of the biggest problems of EEG biometric is the tiny signal-to-noise ratio (SNR) of the signals coupled with a variety of noise sources (Repovs, 2010). To address this noise problem in EEG, we utilize the EEG signal as a feature distribution and computing the dissimilarity measure of EEG distributions with Mallows Distance (Mallows, 1972). To the best of our knowledge, our work is the first to perform stimulus-response based EEG biometric using Mallows Distance. Since Mallows Distance matches distributions in two clusterings in a globally optimal manner and is known to be robust to signal noises, utilizing Mallows Distance allows the matching of the signal distributions in a very natural way. Therefore Mallows Distance provides better performance than other measures (Zhou et al., 2005; Rubner et al., 2000).

We summarize our contributions to three-fold:

- We investigate the feasibility of EEG biometric identification utilizing Mallows Distance in feature distribution’s dissimilarity measure.
- We implement Mallows Distance based EEG identification system with a machine learning algorithm to verify the feasibility of a person identification system with Mallows Distance.
- We evaluate the performance of the implemented identification system to demonstrate the capabilities of a person identification system utilizing Mallows Distance.

This paper is structured as follows: Section 2 provides the details of data acquisition and EEG recording procedures. Section 3 describes the development of our EEG-based personal identification system, which is divided into the following subsections: feature extractions, Mallows Distance, and the classification with SVM. Then, Section 4 provides a description and discussion of the performance evaluation. Lastly, Section 5 concludes the paper.

2 Materials

We utilize the publicly available database from Swartz Center for Computational Neuroscience Foundation (SCCN) to perform EEG-based personal identification via Mallows distance (for Computational Neuroscience Foundation, SCCN).

Before EEG signal data is used toward classification, the data must be labeled with the following information:

- Participant number.
- Stimuli type (target stimuli or non-target stimuli).
- The series of stimuli used toward the participant.

Using Neuroscan software, the collection of multiple channel data are acquired from 10 healthy subjects (six males, four females). Also, this public database has been pre-processed through Neuroscan software to remove any idiosyncrasies that resulted from the recording set-up.

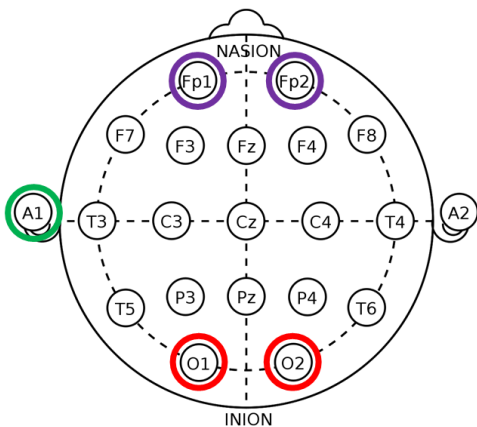


Fig. 1 Standard electrode locations. O1 and O2 is selected as data channel for our dataset.

2.1 Channel Selection

According to Altahtat *et al.* (Altahtat et al., 2015), O2 has the highest channel stability value among 64 channels. Such stability will allow high consistency in terms of repeating signal characteristics over a long period, which is highly preferred. Also, the channel stability of O1 ranked fourth out of 64 channels. These results demonstrate that O1 and O2 are highly recommended EEG channels to be used in biometrics as an alternative to the complete EEG channel set. The position of O1 and O2 is very close to the visual cortex of the brain structure which is responsible for visual input processing. This provides insight to the use of O1 and O2 along with EEG response from the target and non-target stimuli. Examples of target stimuli and non-target stimuli are shown in Fig. 2, each target stimuli have a distinguishable target object in the image, and each non-target stimuli image lacks the main target for focus. Instead of using all-electric brain potentials recorded from 64 electrodes, we selected O1 and O2 (International 10-20 System) electrodes for better computational efficiency and stability over time of our identification system. Moreover, electrode A1 is used as a reference, and Fp1 and Fp2 electrodes are used as grounds (See

Fig. 1). The data acquisition was made at a sampling rate of 1000 Hz, which corresponds to a sample bin of 1 ms, and the impedance was kept below five kOhms. This recording is processed through a SynAmps system coupled with a personal computer (Delorme et al., 2004).

2.2 Experimental Details

While we utilize EEG dataset from SSCN, it is worth to mention that the experimental details from data acquisition from each subject to data preparation for later classification. Each participant performs a categorization task of photographs. Both target and non-target images were equally likely presented in the experiment to eliminate biased from image selection. There were 4 series with 100 images for each series. During each series, participants were instructed to press a touch-sensitive button, and as the eight-bit color photograph flashes, they were told to show their responses following the go and no-go paradigm. When the target image flashes, the participants lift their finger from the button within 1000 ms indicates a go paradigm, and any delay higher than this threshold is considered a no-go response. The image was flashed for only 20 ms to avoid the use of exploratory eye movement. If the image is not a target picture, participants continued to press the button for at least 1000 ms. The stimulus onset asynchrony is 2000 ms. As mentioned above, we organize each task with a series of 100 images with no bias in terms of quantity (i.e., each series consists of 50 target stimuli and 50 non-target stimuli). The target stimuli included pictures of animals, such as mammals, birds, fishes, arthropods, and reptiles as the focal object, while non-target stimuli depicted the natural landscapes or city scenes, pictures of food, fruits, vegetables, and trees in large scale (Delorme et al., 2004). Our study aims to investigate the EEG pattern of individuals responding to the target visual stimulus. Thus, our system selectively employs target pictures as visual stimuli set and then provide a comparison against non-target visual stimuli in evaluation.

3 Methods

We illustrate our implemented system in this section to provide details of our feature extraction methods, distance computation algorithm, and the classification of calculated distances using a linear support vector machine (SVM). The overall identification system framework is shown in Fig. 3 to display the workflow of our identification process.

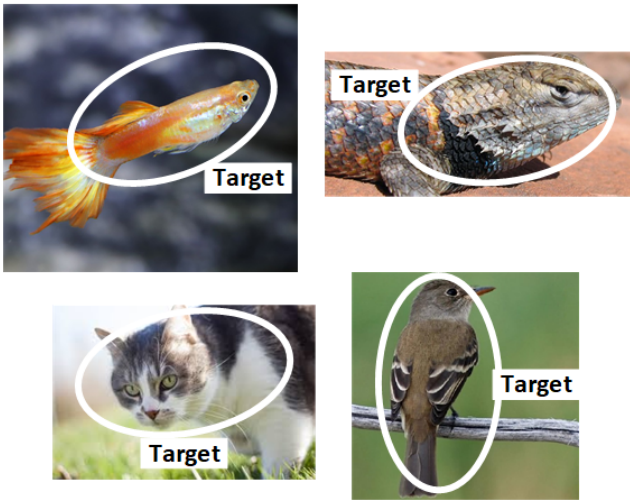
Foremost, we present our Identification Algorithm Illustration to modularize our methodology:

- **EEG Signal Acquisition:** Signal $\rho(t)$ is collected in the temporal domain with t being time. The sampling rate is

Table 1 Five statistical features at the primitive level (Zhang and Sawchuk, 2012)

Statistical features	Definition
Mean	The average value of the signal over the window
Standard Deviation	Measure of dispersion of the signal over the window
Root Mean Square	The quadratic mean of the signal over the window
Average Derivatives	The average of the first order derivatives of the signal over the window
Level Crossing Rate	The total rate of signal crossing the mean level of the signal with a positive slope

Target Stimuli Images



(a) Example of Target Stimuli

Non-Target Stimuli Images



(b) Example of Non-Target Stimuli.

Fig. 2 Examples of both target and non-target stimuli used toward EEG signal acquisition.

determined to be 1000 Hz and the impedance is kept below 5kOhms. The recording is processed with a personal computer through the SynAmps system.

- **Signal Feature Extraction:** Feature set $\phi(n)$ is extracted from $\rho(t)$ with n being total number of features. Mean, standard deviation, root mean square, average derivatives, and level crossing rate at the primitive level is extracted. The scalar values form an array describing the EEG signal.
- **Mallow Distance Calculation:** Mallow distance M is calculated based on the feature set $\phi(n)$.
- **SVM Classification:** Prediction result C from the SVM model is generated using mallow distance M with C .

3.1 Feature Extraction

To capture the unique characteristics of each EEG signal as well as to reduce the dimension of data, we extract feature values from the EEG signal to perform classification.

As shown in Table 2, five statistical features are calculated at the primitive level. Furthermore, we have extracted the EEG feature via an autoregressive (AR) model, discrete wavelet transform, and Fast Fourier Transform (FFT). All eight features of the individual piece are combined to form a single feature distribution.

3.1.1 Autoregressive Model

Since AR models are known to limit the loss of spectral problems and yield the improved frequency resolution compared to the non-parametric approach (Al-Fahoum and Al-Fraihat, 2014), we use AR to extract EEG features. We implement the AR model by calculating the coefficients of the linear system:

$$X_t = \sum_{i=1}^p a_i x_{t-i} + \varepsilon_t, \quad (1)$$

where X_t is the signal at the sampled point t , p is the order of the model, a_i is the AR coefficient, and ε_t is an independent and identically distributed white noise input (Jain and Deshpande, 2004). In our system, the Yule-Walker method was used for AR spectral estimation (Friedlander and Porat, 1984). Before employing the AR model, an optimal order was computed using the Levinson-Durbin method. This method fits an AR model to the auto-correlation sequence of interest and minimizes the model error.

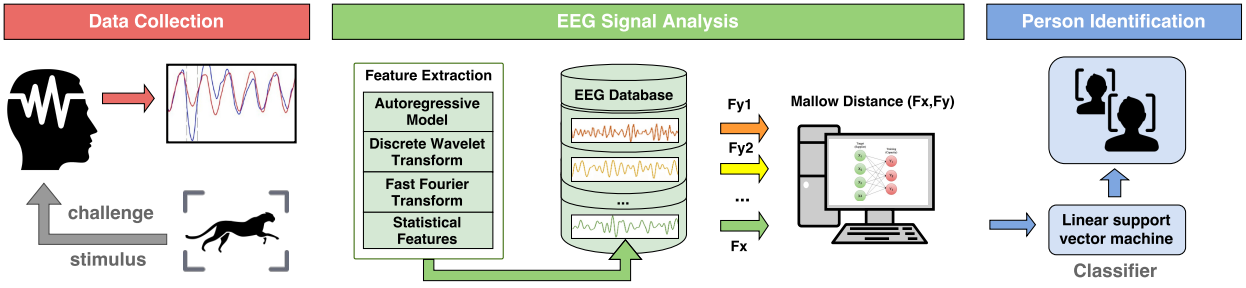


Fig. 3 EEG-based identification system framework, after the EEG signal is collected from subjects using target and non-target visual stimuli, feature extraction is performed to reduce the data dimension. SVM model then performs feature distance computation with Mallows distance and present identification result.

3.1.2 Discrete Wavelet Transform

The wavelet transform is a spectral estimation method in which any function can be written as an infinite series of wavelets. It condenses the time varying signals with many data points into several small parameters that represent the signal (Cvetkovic et al., 2008). Mathematically, the discrete wavelet transform (DWT) of a signal, $x(t)$, is the integral of the signal multiplied by scaled and shifted wavelet function ψ (Ocak, 2009). It is defined by:

$$DWT(j, k) = \frac{1}{\sqrt{|2^j|}} \int_{-\infty}^{\infty} x(t) \psi\left(\frac{t-2^j k}{2^j}\right) dt, \quad (2)$$

where 2^j and $k2^j$ are called the scaling and time location or shifting parameters respectively (Ocak, 2009).

The discrete wavelet transform is particularly suitable for the analysis of sudden and transient signal changes. Since instantaneous visual stimuli elicit our signal, the discrete wavelet transform is suitable for our dataset (Al-Fahoum and Al-Fraihat, 2014).

3.1.3 Fast Fourier Transform

Fast Fourier transform (FFT) is widely used for many applications related to the EEG data analysis and signal processing in general. It quickly computes the discrete Fourier transform (DFT), which reduces the number of computations needed for N points from $2N^2$ to $2N \log N$, where \log is the base-2 logarithm. Consider a complex series $x(k)$ of length N where x is a complex number $x_i = x_{real} + x_{imag}$. Assume that the series outside the range $0, N-1$ is extended N -periodic, where $x_k = x_{k+N}$ for all k (Bourke, 1993). Then, this transform is defined as follows:

$$x_k = \sum_{n=0}^{N-1} x_n \cdot e^{-i2\pi kn/N}. \quad (3)$$

The advantages of implementing the fast Fourier transform are the enhancement of speed over virtually all other available methods for real-time applications and improvement in the performance for the narrow-band signal like our EEG signals (Al-Fahoum and Al-Fraihat, 2014).

3.2 Mallows Distance

After combining the aforementioned features into a cluster with respect to time, we compute the distance between the current cluster and past EEG signal clusters using Mallows distance. Our distance measure has its root in measuring the difference between two multi-variable probability distributions. In 1972, Mallows proposed a Mallows distance to measure the difference between two probability distribution P and Q in R^d with the random variables X and Y (Mallows, 1972). It is defined by a minimum of the expected difference between X and Y overall joint probability distributions F for (X, Y) such that the marginal distribution of X is P and the marginal distribution of Y is Q (Levina and Bickel, 2001):

$$Mallows_p(P, Q) = \min_F \{E_F \|X - Y\|^p\}^{1/p}, \quad (4)$$

subject to:

$$\int_Y dF(X, Y) = P(X), \int_X dF(X, Y) = Q(Y), \quad (5)$$

where p is some value greater or equal to 1. $\|\cdot\|$ indicates the Euclidean length. In theory, Mallows distance can be computed both for discrete or continuous distribution (Levina and Bickel, 2001). Since we formulate the task of matching as a transportation problem between two solid feature set, our distributions are discrete. The discrete distributions:

$$P = \{(x_1, p_1) \cdots (x_m, p_m)\}, 1 \leq i \leq m$$

and

$$Q = \{(y_1, q_1) \cdots (y_n, q_n)\}, 1 \leq j \leq n \quad (6)$$

with the weights add up to 1 ($\sum p_i = 1$ and $\sum q_j = 1$).

The task is to minimize the expectation under the joint distribution $F = (f_{ij})$:

$$E_F \|X - Y\|^p = \sum_{i=1}^m \sum_{j=1}^n f_{ij} \|x_i - y_j\|^p = \sum_{i=1}^m \sum_{j=1}^n f_{ij} d_{ij}, \quad (7)$$

with subject to

$$f_{ij} \geq 0; 1 \leq i \leq m, 1 \leq j \leq n, \quad (8)$$

$$\sum_{j=1}^n f_{ij} = p_i; 1 \leq i \leq m, \quad (9)$$

$$\sum_{i=1}^m f_{ij} = q_j; 1 \leq j \leq n, \quad (10)$$

$$\sum_{i=1}^m \sum_{j=1}^n f_{ij} = \sum_{i=1}^m p_i = \sum_{j=1}^n q_j = 1. \quad (11)$$

In terms of the Earth Mover's Distance (EMD), a special case of the mass transport problem (Rubner et al., 2000), constraint 1 shown in Eq. (8) allows the flow from P to Q but not from Q to P . Since both P and Q are probability distributions with a total mass of 1, weight normalization is not needed. Constraint 2 and 3 shown in Eq. (9) and 10 indicate that the number of supplies that can be sent by the clusters in P is equal to their weights, and the amount of cluster in Q is equal to their weight, respectively. Constraint 4 shown in Eq. (11) matches the clusters in two clusterings in a globally optimal manner. Therefore, it allows the tolerance in the EEG signal noises (Levina and Bickel, 2001).

When Mallows distance is simplified with two samples of the same size $X = \{x_1, \dots, x_n\}$ and $Y = \{y_1, \dots, y_n\}$, the Mallows distance between empirical distribution is:

$$Mallows_p(X, Y) = \left(\frac{1}{n} \min_{(j_1, \dots, j_n)} \sum_{i=1}^n \|x_i - y_{j_i}\|^p \right)^{\frac{1}{p}}, \quad (12)$$

where the minimum is taken over every possible permutations of $\{1, \dots, n\}$ (Levina and Bickel, 2001). This gives every point the weight of $\frac{1}{n}$ resulting equal weighting of every feature. For rapid subject classification, mallows distance have shown potential to execute real-time image annotation in the past (Li and Wang (2008)), this shows the feasibility of using mallows distance for subject classification in real world scenarios under real-time.

3.3 Subject Classification

In order to perform subject classification, we implement a linear SVM to execute multi-class classification.

Linear SVM is a particular linear discriminant classifier, which is known as one of the best classification methods with many computational advantages (Guyon et al., 2002).

With the linear SVM, the points in high dimension feature space are divided into separate categories by a clear gap that is as wide as possible. Then, new sets are mapped to predict which category it belongs to based on which side of the gap they are located (Cortes and Vapnik, 1995).

To strictly test the SVM model and prevent overfitting on existing data, we implement the k -fold cross-validation, with k being 10.

The data set is randomly separated into 10 equal-sized subsets, for each trial, one of 10 subsets is used as a test set and other 9 subsets are used as a training set. Each subset will be treated as a unique class in SVM to obtain the prediction result that enables true positive (TP), true negative (TN), false positive (FP), false negative analysis (FN). This cross-validation is repeated 10 times with each of 10 subsets used exactly once as the validation data. This process occurred separately from channel to channel. Overall, each cross-validation trial data will have 2 channels, and 10 subsets. The resulting model allows rapid subject prediction, per subject prediction duration is determined to be 0.1 seconds from 10 class prediction during each trial of 10-fold cross-validation.

4 Performance Evaluation

4.1 Evaluation Metrics

To examine the effectiveness of utilizing Mallows distance in EEG, we utilize multiple performance metrics for scoring. The metrics include the average accuracy (ACC), balanced accuracy (BAC), f -score ($f-1$), receiver operating characteristics (ROC), and the half total error rate (HTER). Utilizing these metrics, we compare Mallows distance's performance against performance when using DWT and Euclidean distance, and we discuss the results in Sec. 4.4.

4.2 Evaluation Description

In order to perform a systematic performance evaluation, we re-arrange EEG signals into different groups.

A single EEG signal is composed of brainwave responses on 10 visual stimuli. Since each participant experimented on 4 series of the task with 50 target stimuli each, there is a total of 20 EEG samples per person per channel (O1 and O2). Moreover, the performance of each channel is investigated, separately. Thus, with 10 subjects, there is a total of 200 EEG distributions for O1 and 200 EEG distributions for O2. Then, the dissimilarity computation is conducted on EEG distributions of O1 and O2, separately. In other words, one feature distribution from O1 of one subject is selected as a target data, and the rest distributions are considered as a training set. Then, the distance between each target and training pair is computed via Mallows distance. This process repeats for every other 199 distribution. Then, calculated distances undergo the SVM classification with 10-fold cross-validation. This procedure is then repeated for the O2 EEG distributions.

Further, the performance of Mallows distance is compared with the performance of other distances, such as dynamic time warping (DTW) and Euclidean distance (ED). Definition of dynamic time warping for clustering EEG waveform is described in (Huang and Jansen, 1985), and the definition for Euclidean distance on the signals is found in (Helen and Virtanen, 2007).

4.3 Evaluation Results

4.3.1 Accuracy

To measure the system performance, the average accuracy, balanced accuracy, and f -score accuracy are investigated. First accuracy metric, (ACC), is defined as:

$$Accuracy(\%) = \frac{TP + TN}{TP + FP + TN + FN} \quad (13)$$

where TP is a true positive, TN is a true negative, FP is a false positive, and FN is a false negative. Although the ACC assesses the accuracy of the system in a straight forward fashion, the number of negative classes 180, out-weights the number of positive classes 20. This unbalanced number classes can result in negative class heavy biase, which leads to imperfection. Thus, we implement additional metrics for classifier evaluation as follow.

Balanced accuracy metric (BAC) is adopted to handle the class imbalance. By definition, BAC is the arithmetic mean of sensitivity and specificity, and it is known for avoiding inflated performance estimates on the imbalanced dataset.

$$BAC(\%) = \frac{TP}{2(TP + FN)} + \frac{TN}{2(TN + FP)}. \quad (14)$$

Further, we calculate an f -score accuracy measure (f -1) to avoid the class imbalance. It is known as a harmonic mean of precision and recall because the recall and precision are evenly weighted. Mathematically, the f -score is defined as:

$$F_1(\%) = \frac{2TP}{2TP + FP + FN}. \quad (15)$$

The system performance on channel O1 and O2 are summarized in Table. 2 and Fig. 4. The average precision and recall of O1 are 95.90% and 95.50% with ACC of 99.10%, BAC of 97.50%, and f -score of 95.70%. The average precision and recall of O2 are 96.80% and 96.50% with ACC of 99.30%, BAC of 98.06%, and f -score of 96.65%. This implies that using O1 and O2, our system can correctly identify people with the average recall value of 96.00% and the average f -score of 96.18%. As expected, there was a slight discrepancy between ACC and the other two metrics in both O1 and O2 results. Despite the imbalance induced bias toward higher percentage accuracy in terms of ACC for both O1 and

O2, the value alone shows a very similar relationship. In addition, we draw the conclusion that overall TN percentage is higher than TP percentage based on the discrepancy.

The f -score of O2 is higher than that of O1 by 0.95%. However, our system still employs both O1 and O2 because their difference in the accuracy is negligible and several subjects perform better in O1. For instance, subject 6 performs better with O1 than O2 as he achieved higher accuracy for O1 (see Fig. 4(a)) than O2 (see Fig. 4(b)).

Table 2 System performance

Distance Metrics	ACC (%)	BAC (%)	F1 (%)
O1	99.10	97.50	95.70
O2	99.30	98.06	96.65

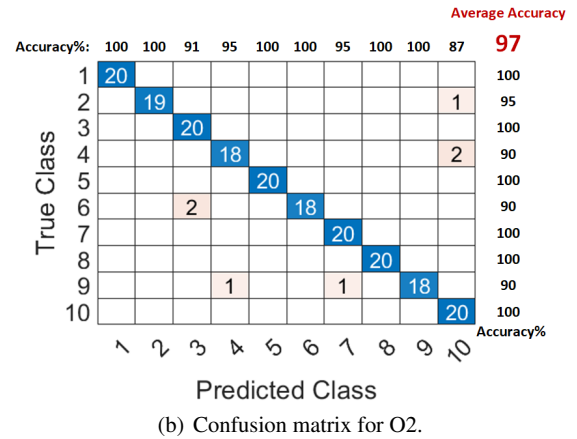
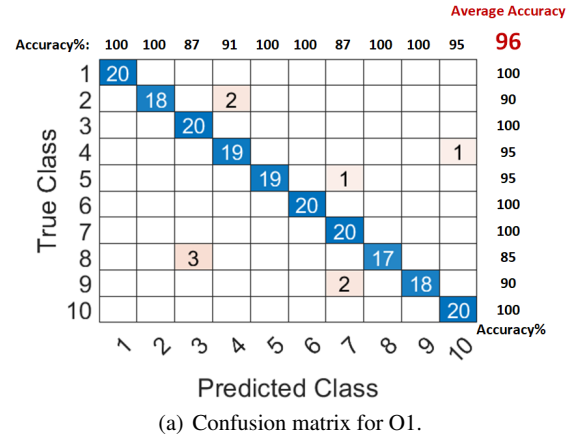
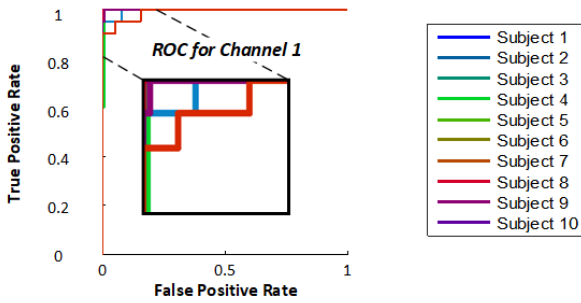


Fig. 4 Classification performance in confusion matrices from channel O1 and O2. Correctly classified subjects are colored in blue, and incorrectly classified subjects are colored in orange. The depth of color signify the rate of occurrence. The rightmost column indicates the recall (%), and the top row presents the precision (%) of each subject. The upper right corner shows the f -score (%).

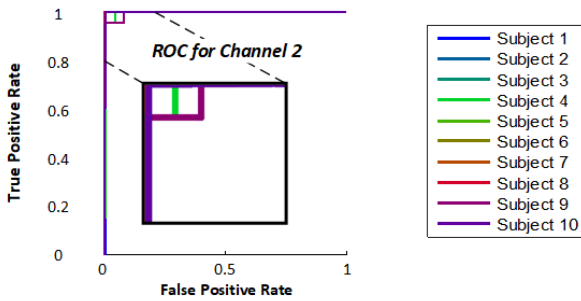
4.3.2 Receiver operating characteristic

For a comprehensive analysis of the system performance, a receiver operating characteristic curve (ROC) is employed to evaluate our system (see Fig. 5(a) and Fig. 5(b)). By definition, ROC visualizes the sensitivity against FPR (false positive rate) as the threshold is varied. If the ROC curve follows the top-left corner of the graph, the system shows high sensitivity and specificity.

Figure 5(a) and Figure 5(b) demonstrate the ROC curves for channel O1 and O2. Two figures illustrate that the performance of the majority of subjects is similar except for subject 8. The curve of subject 8 is slightly lower for O1, and this complies with the result shown in Fig. 4(a). Overall, most ROC curves follow the top-left corner of the graph, signifying that our system is robust and feasible.



(a) The average ROC curves of 10 subjects on Channel O1.



(b) The average ROC curves of 10 subjects on Channel O2.

Fig. 5 Receiver operating characteristic curves with 10 subjects. Close-up images are also shown.

4.3.3 Half total error rate

Half total error rate (HTER) is a way to measure the detection performance, which is popularly used as accuracy metrics for biometrics identification. HTER is defined in the following formula:

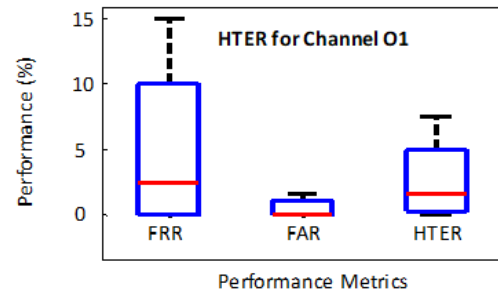
$$HTER = \frac{FAR + FRR}{2} [\%], \quad (16)$$

where FAR refers to the false accept rate, and FRR indicates the false rejection rate.

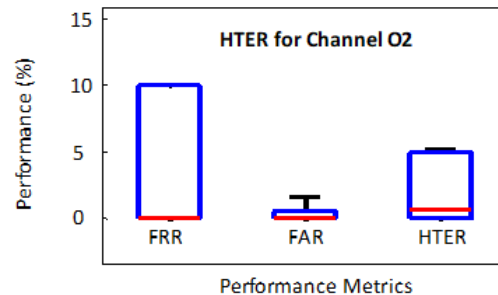
Figure 6(a) illustrates the FRR, FAR, and HTER of 10 subjects on channel O1. The error bar represents the standard deviation of each metric, and the red line in the box indicates the median value. The average FRR and FAR value for O1 are 4.500% and 0.501% with the standard deviation of 5.503% and 0.716%. When averaging two values, we achieved the HTER value of 2.501% with the standard deviation of 2.599%.

Figure 6(b) shows the FRR, FAR, and HTER for channel O2. The average FRR and FAR value for 10 subjects on O2 are 3.500% and 0.390% with the standard deviation of 4.743% and 0.590%, respectively. HTER value for O2 is 1.945% with its standard deviation of 2.295%. Therefore, the overall performance of our system using both O1 and O2 achieves the FRR of 4.000%, FAR of 0.446%, and HTER of 2.223%. For both O1 and O2, FAR is much lower than FRR because our negative class outnumbered the positive class.

Compared to the performance of O2, O1 provides higher FRR, FAR, and HTER by 1.000%, 0.740%, and 0.556%. This result suggests that using signal from O2 channel would make classification less prone to error than O1. However, as addressed above, both channels are used for the system because the performance of an individual varies from channel to channel. In conclusion, this result shows that the FRR is significantly higher than FAR in Figure 6, maximizing the security of the system that adapts this method.



(a) Boxplot of FRR, FAR, and HTER for channel O1.



(b) Boxplot of FRR, FAR, and HTER for channel O2.

Fig. 6 Boxplot for channel O1 and O2. The red line indicates the median value among 10 subjects. The standard deviation is represented by the error bars in black color.

4.4 Comparison with other distance metrics

In order to illustrate performance gain in classification accuracy utilizing Mallows distance, we exhibit the classification performance in different distance metrics.

Table 3 shows a summary of the performance measures of Mallows distance, dynamic time warping (DTW), and Euclidean distance. The testing performance of Mallows distance is found to be satisfactory compared to that of DTW and Euclidean distance. Specifically, the f -score of Mallows distance is higher than that of DTW and Euclidean distance by 2.31% and 6.48%, respectively. This proves that there is a significant performance advantage for adopting Mallows distance over DTW and Euclidean distance.

Table 3 Performance Comparison

Distance Metrics	ACC (%)	BAC (%)	FI (%)
Mallows	99.20	97.78	96.18
DTW	97.60	94.23	93.87
Euclidean	94.82	90.88	89.70

Although Euclidean distance has the advantage of being simple and fast in computation, it is unreliable when one of the features has a relatively large quantity and overpowers the other. The inevitable imbalance of feature weight weakens the accuracy of using Euclidean distance. Due to this weakness, Euclidean distance demonstrates the lowest performance as shown in Table. 3. On the other hand, DTW allows two-time series that are similar but locally out of phase to align in a non-linear manner, thereby resolves the problem of Euclidean distance (Ratanamahatana and Keogh, 2004). Still, DTW algorithm is inevitable from one critical problem; it may not detect obvious alignments in two signal if a feature of one signal is slightly higher or lower than its corresponding feature of the other signal (Ben Ali et al., 2015; Keogh and Pazzani, 2001). Thus, DTW is vulnerable to noises and provides less accuracy than Mallows distance. Mallows distance, which uses a clustering comparison, is robust to the signal noises and shows a better performance than two metrics in a statistical manner. Thus, Mallows distance is suitable for EEG-based subject identification.

4.5 Impact of stimuli types

In this section, we investigate the performance of the EEG responses generated by non-target stimuli with 10 participants. Table 4 summarizes the average performance (O1 and O2) with FRR, FAR, and HTER for target and non-target

Table 4 Error rates for target and non-target stimulus

Type	FRR (%)	FAR (%)	HTER (%)
Target	4.000	0.446	2.223
Non-target	6.250	0.695	3.473

stimuli. When the target stimuli are employed, the average FRR and FAR value are 4.000% and 0.446% with the standard deviation of 5.026% and 0.641%, respectively. Therefore, the EEG signals that are generated by target stimuli provide the HTER of 2.223% with the standard deviation of 2.4029%. When EEG signals are evoked by non-target stimuli, our system achieves the FRR of 6.250%, FAR of 0.695% and HTER of 3.473% with the standard deviation of 7.927%, 0.968% and 4.125%, correspondingly. For both target and non-target, the horizontal line in the box plots for FRR and FAR is absent because their median value for FRR and FAR is 0. Performance comparison between target and non-target stimuli are illustrated in Fig. 7. In general, FRR, FAR and HTER of the target stimulation are lower than FRR, FAR and HTER of the non-target stimulation by 2.250%, 0.249%, and 1.250%. Thus, the stimulation of target images provides better performance than the presentation of non-target images. This result suggests that the target stimuli generate more distinguishable EEG responses than the non-target stimuli during the categorization task.

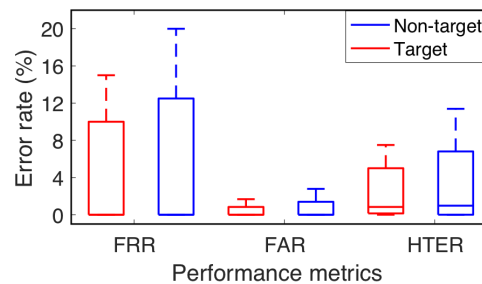


Fig. 7 Boxplot of FRR, FAR, and HTER with target and non-target stimuli. The horizontal line in the box indicates the median value, and error bar represents the standard deviation.

5 Conclusion

In this paper, we presented a stimulus-response based EEG biometric using Mallows distance. Unlike previously published works, we utilize Mallows distance calculation for the EEG signal cluster model in the personal identification process. We first investigate and apply Mallow distance to EEG signal from healthy participants in the existing database. We then extract statistical features, perform autoregressive model, discrete wavelet transform, and fast Fourier transform for data dimension reduction. Then, we employ an SVM model to perform EEG feature distribution classification that validates the reliability of using Mallows Distance in EEG based personal identification. Furthermore, we perform an extensive performance evaluation, which presents a classification accuracy of 96.18%. As a result, EEG biometric with Mallows distance to compute feature distance shows promising results and is highly feasible for future applications.

Acknowledgement

This work is in part supported by the United States National Science Foundation(NSF) under grant No. 1564104/1840790.

References

- Al-Fahoum AS, Al-Fraihat AA (2014) Methods of eeg signal features extraction using linear analysis in frequency and time-frequency domains. *ISRN neuroscience* 2014
- Altahat S, Wagner M, Marroquin EM (2015) Robust electroencephalogram channel set for person authentication. In: 2015 IEEE International Conference on Acoustics, Speech and Signal Processing (ICASSP), IEEE, pp 997–1001
- Beenau BW, Bonalle DS, Fields SW, Gray WJ, Larkin C, Montgomery JL, Saunders PD (2006) Method and system for dna recognition biometrics on a fob. US Patent 7,121,471
- Ben Ali B, Masmoudi Y, Dhouib S (2015) Accurate and fast dynamic time warping approximation using upper bounds. In: *Telecommunications and Signal Processing (TSP), 2015 38th International Conference on*, IEEE, pp 1–6
- Bourke P (1993) Dft (discrete fourier transform) fft (fast fourier transform). Internet, <http://astronomy.swin.edu.au/~pbourke/analysis/dft>
- Brumback CB, Myers NA, Yuen SGJ, Park J, Diemer TS (2015) Biometric monitoring device with heart rate measurement activated by a single user-gesture. US Patent 9,042,971
- for Computational Neuroscience Foundation (SCCN) SC (2013) Eeg/erp data available for free public download. Last accessed 10 April 2016
- Cortes C, Vapnik V (1995) Support-vector networks. *Machine learning* 20(3):273–297
- Cvetkovic D, Übeyli ED, Cosic I (2008) Wavelet transform feature extraction from human ppg, ecg, and eeg signal responses to elf pemf exposures: A pilot study. *Digital signal processing* 18(5):861–874
- Delorme A, Rousset GA, Macé MJM, Fabre-Thorpe M (2004) Interaction of top-down and bottom-up processing in the fast visual analysis of natural scenes. *Cognitive Brain Research* 19(2):103–113
- Friedlander B, Porat B (1984) The modified yule-walker method of arma spectral estimation. *IEEE Transactions on Aerospace and Electronic Systems* (2):158–173
- Gui Q, Jin Z, Xu W (2014a) Exploring eeg-based biometrics for user identification and authentication. In: 2014 IEEE Signal Processing in Medicine and Biology Symposium (SPMB), IEEE, pp 1–6
- Gui Q, Jin Z, Xu W (2014b) Exploring EEG-based Biometrics for User Identification and Authentication. In: the IEEE Signal Processing in Medicine and Biology Symposium (SPMB'14), Philadelphia, Pennsylvania, USA, pp 1–6
- Gui Q, Jin Z, Blondet MR, Laszlo S, Xu W (2015a) "towards eeg biometrics: Pattern matching approaches for user authentication". In: *IEEE International Conference on Identity, Security and Behavior Analysis (ISBA'15)*, Kong Hong, pp 1–7
- Gui Q, Jin Z, Blondet MVR, Laszlo S, Xu W (2015b) Towards eeg biometrics: Pattern matching approaches for user identification. In: *IEEE International Conference on Identity, Security and Behavior Analysis (ISBA 2015)*, IEEE, pp 1–6
- Gui Q, Jin Z, Xu W, Ruiz-Blondet MV, Laszlo S (2015c) Multichannel eeg-based biometric using improved rbf neural networks. In: 2015 IEEE Signal Processing in Medicine and Biology Symposium (SPMB), pp 1–6
- Guyon I, Weston J, Barnhill S, Vapnik V (2002) Gene selection for cancer classification using support vector machines. *Machine learning* 46(1-3):389–422
- Hazarika N, Chen JZ, Tsoi AC, Sergejew A (1997) Classification of eeg signals using the wavelet transform. In: *Digital Signal Processing Proceedings, 1997. DSP 97.*, 1997 13th International Conference on, IEEE, vol 1, pp 89–92
- Helen M, Virtanen T (2007) Query by example of audio signals using euclidean distance between gaussian mixture models. In: *Acoustics, Speech and Signal Processing, 2007. ICASSP 2007. IEEE International Conference on*, IEEE, vol 1, pp I-225
- Huang HC, Jansen B (1985) Eeg waveform analysis by means of dynamic time-warping. *International journal of bio-medical computing* 17(2):135–144
- Jain A, Hong L, Bolle R (1997) On-line fingerprint verification. *IEEE transactions on pattern analysis and machine intelligence* 19(4):302–314
- Jain AK, Nandakumar K, Nagar A (2008) Biometric template security. *EURASIP Journal on advances in signal processing* 2008:113
- Jain S, Deshpande G (2004) Parametric modeling of brain signals. In: *Biotechnology and Bioinformatics, 2004. Proceedings. Technology for Life: North Carolina Symposium on*, IEEE, pp 85–91
- Juel-Nielsen N, Harvald B (1958) The electroencephalogram in uniovular twins brought up apart. *Human Heredity* 8(1):57–64
- Keogh EJ, Pazzani MJ (2001) Derivative dynamic time warping. In: *Sdm, SIAM*, vol 1, pp 5–7
- Levina E, Bickel P (2001) The earth mover's distance is the mallows distance: some insights from statistics. In: *Computer Vision, 2001. ICCV 2001. Proceedings. Eighth IEEE International Conference on*, IEEE, vol 2, pp 251–

- Li J, Wang JZ (2008) Real-time computerized annotation of pictures. *IEEE transactions on pattern analysis and machine intelligence* 30(6):985–1002
- Li Z, Wang Y, Rathore AS, Song C, Nyayapathi N, Vu T, Xia J, Xu W (2018) Pavessel: Practical 3d vessel structure sensing through photoacoustic effects with its applications in palm biometrics. *Proc ACM Interact Mob Wearable Ubiquitous Technol* 2(3):122:1–122:24, DOI 10.1145/3264932, URL <http://doi.acm.org/10.1145/3264932>
- Lin F, Song C, Zhuang Y, Xu W, Li C, Ren K (2017) Cardiac scan: A non-contact and continuous heart-based user authentication system. In: *Proceedings of the 23rd Annual International Conference on Mobile Computing and Networking*, ACM, New York, NY, USA, MobiCom '17, pp 315–328
- Lin F, Cho KW, Song C, Xu W, Jin Z (2018) Brain password: A secure and truly cancelable brain biometrics for smart headwear. In: *Proceedings of the 16th Annual International Conference on Mobile Systems, Applications, and Services*, ACM, New York, NY, USA, MobiSys '18, pp 296–309
- Luo S, Nguyen A, Song C, Lin F, Xu W, Yan Z (2019) Oculock: Exploring human visual system for authentication in virtual reality head-mounted display
- Mallows CL (1972) A note on asymptotic joint normality. *The Annals of Mathematical Statistics* 43(2):508–515, URL <http://www.jstor.org/stable/2239988>
- Mohammadi G, Shoushtari P, Molaee Ardekani B, Shamsollahi MB (2006) Person identification by using ar model for eeg signals. In: *Proceeding of World Academy of Science, Engineering and Technology*, vol 11, pp 281–285
- Ocak H (2009) Automatic detection of epileptic seizures in eeg using discrete wavelet transform and approximate entropy. *Expert Systems with Applications* 36(2):2027–2036
- Patil OR, Wang W, Gao Y, Xu W, Jin Z (2018) A non-contact ppg biometric system based on deep neural network. In: *2018 IEEE 9th International Conference on Biometrics Theory, Applications and Systems (BTAS)*, IEEE, pp 1–7
- Poulos M, Rangoussi M, Alexandris N, Evangelou A, et al. (2002) Person identification from the eeg using nonlinear signal classification. *Methods of information in Medicine* 41(1):64–75
- Raja KB, Raghavendra R, Vemuri VK, Busch C (2015) Smartphone based visible iris recognition using deep sparse filtering. *Pattern Recognition Letters* 57:33–42
- Ratanamahatana CA, Keogh E (2004) Everything you know about dynamic time warping is wrong. In: *Third Workshop on Mining Temporal and Sequential Data*, Citeseer
- Rathore AS, Zhu W, Daiyan A, Xu C, Lin F, Wang K, Xu W (2020) Sonicprint: A generally adoptable and secure fingerprint biometrics in smart devices. In: *Proceedings of the 18th Annual International Conference on Mobile Systems, Applications, and Services*, ACM, Toronto, Canada
- Repovs G (2010) Dealing with noise in eeg recording and data analysis. In: *Informatica Medica Slovenica*, vol 15, pp 18–25
- Rubner Y, Tomasi C, Guibas LJ (2000) The earth mover's distance as a metric for image retrieval. *International journal of computer vision* 40(2):99–121
- Song C, Wang A, Ren K, Xu W (2016) Eyeveri: A secure and usable approach for smartphone user authentication. In: *IEEE INFOCOM 2016-The 35th Annual IEEE International Conference on Computer Communications*, IEEE, pp 1–9
- Subasi A (2007) Eeg signal classification using wavelet feature extraction and a mixture of expert model. *Expert Systems with Applications* 32(4):1084–1093
- Tian Y, Li Y, Liu X, Deng RH, Sengupta B (2018) Pribioauth: Privacy-preserving biometric-based remote user authentication. In: *2018 IEEE Conference on Dependable and Secure Computing (DSC)*, IEEE, pp 1–8
- Wang Y, Li Z, Vu T, Nyayapathi N, Oh KW, Xu W, Xia J (2018) A robust and secure palm vessel biometric sensing system based on photoacoustics. *IEEE Sensors Journal* 18(14):5993–6000
- Zhang M, Sawchuk AA (2012) Motion primitive-based human activity recognition using a bag-of-features approach. In: *Proceedings of the 2Nd ACM SIGHT International Health Informatics Symposium*, ACM, New York, NY, USA, IHI '12, pp 631–640, DOI 10.1145/2110363.2110433, URL <http://doi.acm.org/10.1145/2110363.2110433>
- Zhang Y, Zhang Y, Lo B, Xu W (2020) Wearable eeg signal processing for automated cardiac arrhythmia classification using cfase-based feature selection. *Expert Systems* 37(1):e12432
- Zhou D, Li J, Zha H (2005) A new mallows distance based metric for comparing clusterings. In: *Proceedings of the 22nd international conference on Machine learning*, ACM, pp 1028–1035
- Zhuang Y, Song C, Lin F, Li Y, Li C, Xu W (2016) On the feasibility of non-contact cardiac motion sensing for emerging heart-based biometrics. In: *2016 IEEE Radio and Wireless Symposium (RWS)*, IEEE, pp 204–206



Baicheng Chen is an undergraduate student in the State University of New York (SUNY) at Buffalo, where he is a member of the Embedded Sensing and Computing (ESC) lab lead by Dr. Wenyao Xu.



Kun Woo Cho is a Ph.D. student in the Department of Computer Science at the Princeton University, under the direction of Dr. Kyle Jamieson in the Princeton Advanced Wireless Systems Lab.



Chenhan Xu is a Ph.D. student in the Dept. of Computer Science and Engineering, SUNY Buffalo working under the guidance of Dr. Wenyao Xu at the Embedded Sensing and Computing (ESC) Lab.



Zhengxiong Li is a Ph.D. candidate in the Department of Computer Science at the State University of New York at Buffalo, under the direction of Prof. Wenyao Xu at the Embedded Sensing and Computing (ESC) Lab.



Dr. Feng Lin is a senior researcher and Ph.D. advisor in Zhejiang University (ZJU). He co-directed the Embedded Sensing and Computing (ESC) lab in the State University of New York at Buffalo. He received his Ph.D. degree from the Department of Electrical and Computer Engineering at Tennessee Technological University.



Dr. Zhanpeng Jin is an Associate Professor of Computer Science and Engineering Department in the State University of New York (SUNY) at Buffalo, where directs the CyberMed Group. He was a Postdoctoral Research Associate at the University of Illinois at Urbana-Champaign (UIUC) and received his Ph.D. degree in Electrical Engineering from the University of Pittsburgh (2010).



Dr. Wenyao Xu is an Associate Professor of Computer Science and Engineering Department in the State University of New York (SUNY) at Buffalo, where he founds and directs the ESC (Embedded Sensing and Computing) Group. He has published over 160 technical papers, co-authored 2 books and is a named inventor on many international and U.S. patents. He received the Ph.D. degree from University of California, Los Angeles (UCLA) in 2013.